Magnetism of 3d transition-metal monolayers on Rh(100)

A. Al-Zubi,[*] G. Bihlmayer,[†] and S. Blügel

Institut für Festkörperforschung and Institute for Advanced Simulation, Forschungszentrum Jülich and
JARA, D-52425 Jülich, Germany

We employ the full-potential linearized augmented plane-wave method to report a systematic density-functional theory study of the magnetic properties of the 3d transition-metal (V, Cr, Mn, Fe, Co, and Ni) monolayers deposited on the Rh(100) substrate. We find that all monolayer films are magnetic. The size of the local magnetic moments across the transition-metal series follows Hund's rule with a maximum magnetic moment of $3.77\mu_B$ for Mn. The largest induced magnetic moment of about $0.46\mu_B$ was found for Rh atoms adjacent to the Co film. When relaxations are included, we predict a ferromagnetic (FM) ground state for V, Co, and Ni, while Cr, Mn, and Fe favor a $c(2 \times 2)$ antiferromagnetic (AFM) state, a checkerboard arrangement of up and down magnetic moments. The magnetic anisotropy energies of these ultrathin magnetic films are calculated for the FM and AFM states. With the exception of Cr, the easy axis of the magnetization is predicted to be in the film plane. Rough estimates of the ordering temperatures are given. To gain an understanding of the $c(2 \times 2)$ AFM state of Fe/Rh(100), we analyze this result with respect to the trends of the magnetic order of 3d monolayers on other 4d substrates, such as Pd(100) and Ag(100).

PACS number(s): 75.70.Ak, 71.15.Mb, 73.20.−r

I. INTRODUCTION

During the past two decades, theoretical and experimental investigations were performed to understand the magnetism of ultrathin magnetic films on (100) oriented nonmagnetic substrates. Mainly the weakly interacting coinage metals (Cu, Ag, Au) and some transition metals (TMs), for example, Pd, have been chosen as substrates in order to minimize the interaction between monolayer and substrate.[1,2] Cu with an experimental lattice constant of $a_0 = 3.61$ Å turned out to be an ideal template for fcc bulk TMs, while Ag ($a_0 = 4.09$ Å) and Au ($a_0 = 4.08$ Å) are templates to grow bcc metals. Employing density functional theory (DFT), some general trends were identified for 3d monolayers (MLs) on these substrates: (i) The magnetic moments of the monolayers are considerably enhanced as compared to the equivalent bulk systems and, (ii) similar to the bulk cases, Fe, Co, and Ni are ferromagnetic (FM) on these substrates, while V, Cr, and Mn prefer a $c(2 \times 2)$ antiferromagnetic (AFM) structure (i.e., a checkerboard arrangement of antiparallel magnetic moments,[3,4]) a magnetic structure that cannot be derived from respective bulk phases. Experimentally, Ortega and Himpsel studied 3d monolayers on Ag(100) and confirmed the theoretical predictions, most notably the magnetism of V on Ag(100).[5]

More recently, the field has taken a different turn, moving away from monolayers on weakly interacting substrates to those on 4d and 5d transition-metal ones. This is motivated by a couple of unexpected findings, which include the prediction of a ferromagnetic phase for the prototype antiferromagnet Cr,[6] the prediction[6–9] and experimental verification of the $c(2 \times 2)$ AFM phase for Fe,[10] the prediction of $c(2 \times 2)$ AFM Co,[6] and the discovery of a homochiral cycloidal magnetic phase for Mn (Refs. 11,12), all as monolayers on W(100). Signs of magnetic frustration have been reported from calculations of Fe/Mn alloys on W(001) (Ref. 13) and also Fe/Ir(001) was found to be close to a transition from FM to AFM coupling, depending on the relaxation of the overlayer.[14] Experimentally and theoretically, a complex long-ranged magnetic structure of an Fe monolayer on Ir(111) has been observed.[15]

These findings motivate a more systematic investigation of monolayers on 4d and 5d substrates in general. In this paper we investigate 3d monolayers on the 4d TM substrate Rh(100). Rh has a large Stoner enhanced susceptibility, as shown for Rh films on Fe (Ref. 16), and FeRh is known to form ordered alloys in the cesium chloride (CsCl-type) structure with subtle magnetic properties.[17–19] The lattice constant of Rh ($a_0 = 3.80$ Å) is in between those of Cu and Ag and thus Rh serves as a potential substrate to grow artificial phases of 3d transition-metal films such as fcc Fe stabilized under tensile strain or bcc Co under compressive strain. The Rh(001) substrate provides favorable growth conditions for transition-metal films despite a large lattice mismatch of fcc Fe or Co and bcc Fe with Rh of about 6%, 8%, and −7%, respectively. For example, no notable intermixing has been encountered at the interface of Fe/Rh(100) during growth of Fe films.[20] Epitaxial, pseudomorphic layer-by-layer growth of one and two layers of Co on Rh(100) was reported by Begley *et al.*,[21] and several groups[20,22–24] have been able to grow pseudomorphically even thicker films of face-centered tetragonal Fe on Rh(100). Recent reports show that FeCo alloys can be grown on Rh(100) where the composition of the alloy can be used to tailor the magnetic anisotropy of the system.[25] Moreover, the same group used Rh(100) spacers to achieve a FM or AFM interlayer exchange coupling depending on the Rh thickness.[26]

Hayashi *et al.*[23,24] concluded on the basis of soft x-ray magnetic circular dichroism experiments measured at room temperature that a monolayer and a bilayer of Fe are not ferromagnetic and interpreted them as magnetically dead, caused by the large strain exerted in the interface of the thin film and the substrate. Hwang *et al.*[27] found experimentally a suppression of the ferromagnetic order of Fe overlayers on the Rh(100) surface, and they as well as Spisak and Hafner[28] predicted a $c(2 \times 2)$ AFM order for one ML Fe on Rh(100) on the basis of DFT calculations.

We study the chemical trend of the interlayer relaxation, the magnetic moments and structure, the magnetic anisotropy energy (MAE), and the magnetization direction across the

transition-metal series of $3d$ MLs on Rh(100). We calculate the spin-orbit and dipole-dipole contribution to the MAE and together with the energy difference between the FM and AFM states we estimate the Néel and Curie temperatures of uniaxial antiferromagnets and ferromagnets, respectively. The results on the electronic and magnetic properties are compared to previous theoretical studies on $4d$ metal substrates such as Pd(100) (Ref. 3) and Ag(100).[4] Since the d band of the substrate is filled by one additional electron when comparing Rh ($a_0 = 3.80$ Å) to Pd ($a_0 = 3.89$ Å) and Pd to Ag ($a_0 = 4.09$ Å), and the lattice constant increases by about 2.5% each, the comparison of the results of the $3d$ TM MLs on these substrates allows an efficient analysis of the role of different in-plane lattice constants, the hybridization between $3d$ and $4d$ orbitals, and the charge transfer across the $3d/4d$ interface for the magnetic properties in these films. In particular, from a comparison of the non-, ferro-, and antiferromagnetic densities of states (DOS) of Fe on Rh, Ag, or Pd, we elucidate the mechanisms that drive the Fe ML into the antiferromagnetic state on Rh. Moreover, we compare this system with Cr on Rh to explore the trends through the TM series and to understand the role of hybridization on the magnetic order.

II. METHOD

We determined the structural, electronic, and magnetic properties of $3d$ TM monolayers on Rh(100) by performing first-principles calculations using the full-potential linearized augmented plane-wave (FLAPW) method[29] in film geometry as implemented in the FLEUR code.[30] The generalized-gradient approximation of Perdew, Burke, and Ernzerhof was applied,[31] leading to a Rh bulk lattice constant of 3.819 Å, which is only 0.4% larger than the experimental lattice constant of 3.804 Å.[32]

The film was modeled by a symmetric seven-layer Rh(100) slab covered by a single $3d$ monolayer on each side, using the calculated Rh in-plane lattice constant. Relaxations were considered for the topmost two layers, that is, the $3d$ ML and the interface layer Rh(I).

Both the FM and the $c(2 \times 2)$ AFM configuration were relaxed. We used about 120 LAPW basis functions per atom with a muffin-tin radius of 1.22 Å for the $3d$ monolayer atoms and 1.28 Å for the Rh atoms. The irreducible part of the two-dimensional Brillouin zone (I2DBZ) was sampled with 78 $\mathbf{k}_\parallel$ points to determine the relaxations and the energy differences between the different magnetic configurations with the same $c(2 \times 2)$ unit cell. For the calculations of the MAE, spin-orbit coupling (SOC) was included in the Hamiltonian and 1024 $\mathbf{k}_\parallel$ points were used in the full 2DBZ. Tests with 4096 $\mathbf{k}_\parallel$ points for selected systems confirmed convergence with respect to this parameter. For these calculations the force theorem[33] was employed, but the potential was converged including SOC, although with less dense sampling of the reciprocal space.

III. RESULTS

A. Relaxations and magnetic moments

We calculated the relaxations between the layers i and j, Δd_{ij}, defined as

$$\Delta d_{ij} = \frac{d_{ij} - d_0}{d_0}, \qquad (1)$$

where d_{ij} is the spacing between the layers i and j, and d_0 is the ideal bulk interlayer distance of the substrate.

The relaxations of the interlayer spacing between the $3d$ monolayer and the topmost substrate layer, Δd_{12}, and the first Rh interlayer spacing, Δd_{23}, are presented in Fig. 1 for both FM and AFM configurations. As a global trend we find that, as a function of the $3d$ band filling, the interlayer relaxation between the first and second Rh layer is reduced from a 7% tetragonal expansion for V at the beginning of the series to the almost ideal bulk interlayer spacing for the Ni monolayer at the end of the series.

Analyzing Δd_{12}, we notice that for the FM configuration the smallest inward relaxation of the $3d$ monolayers occurs for Mn and Fe on Rh(100), where the magnetovolume effect is strongest; that is, the large magnetic moments (see Fig. 2) of these TMs compensate the strong inward relaxation—caused by the larger Rh lattice constant—most efficiently. Of course, there are also other factors controlling Δd_{12}; for example, for V the relaxation is smaller than for Cr, although the magnetic moment of the latter is much larger than that of vanadium. Here also the fact that the bulk lattice constant of V is 5% larger than that of Cr has to be considered.

Comparing our results to data existing in the literature, we notice that the relaxations in Fig. 1 for Fe/Rh(100) are stronger than in the calculation of Hwang *et al.*,[27] which reported -2.8% and -9.4% contraction of the first interlayer distance for FM and AFM order, respectively. Since they used a methodology similar to ours, the difference has to originate from the relaxations of the deeper layers, which were ignored in Ref. 27. Indeed, in another *ab initio* calculation for this surface, including multilayer relaxations, values for Δd_{12} of -7.2% and -12.6% were obtained for FM and AFM order, respectively,[28] in good agreement with the data from Fig. 1. Also, the values for Δd_{23} agree within 0.2%. Experimentally, low-energy electron diffraction measurements by Begley and collaborators [34] reported a relaxation of $\Delta d_{12} = -8.4 \pm 1.6\%$. Taking temperature effects and uncertainties in the determination of the exact Fe coverage into account, the agreement is
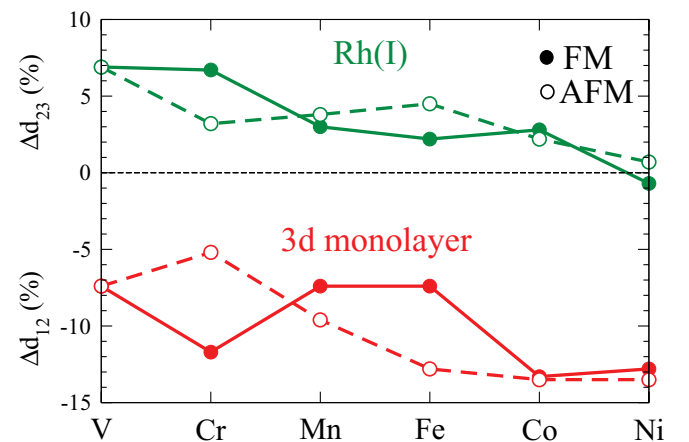

FIG. 1. (Color online) Relaxations of the first and second interlayer spacing, Δd_{12} and Δd_{23}, respectively, for $3d$ TM monolayers on Rh(100) for the FM and the $c(2 \times 2)$ AFM configuration. The corresponding changes are given with respect to the substrates' bulk interlayer spacing, which is 1.91 Å.
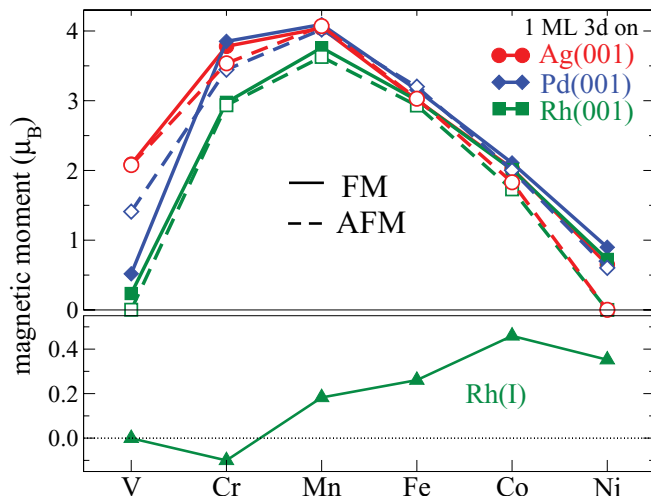
FIG. 2. (Color online) Magnetic moments of (top) 3*d* TM monolayers on Ag, Pd, and Rh(100) surfaces and (bottom) the interface Rh moments. The TM moments are denoted by solid (open) symbols for the FM (AFM) solutions. For the FM case, the magnetic moment of the interface Rh atoms is given by solid (green) squares. The data for the 3*d* TMs on Ag(100) and Pd(100) are taken from Refs. [3] and [4].

quite reasonable. The same authors reported slightly smaller relaxations of $-6.8 \pm 1.6\%$ for Co on the Rh(100) surface,[21] while our calculations indicate even stronger relaxations for the Co films, quite independent of the magnetic order.

With the exception of Ni, in all cases the equilibrium distance between the interface Rh layer and the bulk Rh underneath, Δd_{23}, increases with respect to the substrates' bulk interlayer spacing. Moving from left to right through the periodic table, we find that Δd_{23} decreases, supporting the interpretation that the *d*-band filling controls these relaxations.[35,36] This highlights the importance of multilayer relaxations for the early transition monolayers. The same trend can be seen for the monolayers with $c(2 \times 2)$ AFM configuration: while Δd_{12} is also influenced by the magnetic moment of the 3*d* monolayer, Δd_{23} depends almost solely on the *d*-band filling.

In Fig. 2 the magnetic moments of the 3*d* TM monolayers on Rh(100) are compared with the Ag(100) and Pd(100) substrates for the FM and AFM structures at the relaxed interlayer distances. The magnetic moments on Rh(100) are smaller than those on Ag(100) or Pd(100) for the early TMs, whereas they are quite similar for the late TMs. This can be understood on the basis of the observation that the overlap of the *d* wave functions with the substrate is larger for the early TMs than for the late TMs. Therefore, the dependence of the TM magnetic moments on the chosen substrate is largest at the beginning of the TM series. The largest moment, in all cases, is found for Mn. The V and Ni magnetic moments vanish for the $c(2 \times 2)$ AFM structure.

For FM order of the 3*d* metal, the induced magnetic moment of the Rh interface layer couples antiferromagnetically with Cr and ferromagnetically with Mn, Fe, Co, and Ni, whereas almost no moment is induced by V. The largest induced magnetic moment is caused by the Co monolayer. The large value of $0.46\mu_B$ on the Rh atom agrees with the values found for

Co/Rh(100) multilayers.[37] However, in these experiments even larger Rh moments were reported for Fe/Rh(100) multilayers. In fact, our value of $0.27\mu_B$ on Rh for Fe/Rh(100) agrees nicely with previous theoretical results;[28] the reasons for the deviation from experiments might come from the multilayer structure. For Fe, Co, and Ni layers, the induced moments in the deeper Rh layers show an oscillatory AFM and FM coupling that is qualitatively in line with the observed interlayer exchange coupling.[26] The induced moments are much larger for Rh than for substrates like Ag(100), highlighting the importance of the substrate for magnetic properties like the magnetic anisotropy, which is discussed below. Of course the AFM ordered TM films induce no magnetic moment in the interface Rh layer, and the induced moments in the deeper layers are considerably smaller and coupled antiferromagnetically to the nearest 3*d* monolayer atoms.

B. Magnetic order

The total energy difference $\Delta E = E_{AFM} - E_{FM}$ between the $c(2 \times 2)$ AFM and the FM configuration is plotted in Fig. 3 for the 3*d* TM monolayers on different substrates. For the Rh(100) substrate, we found a FM ground state for V, Co, and Ni, while it is $c(2 \times 2)$ AFM for Cr, Mn, and Fe. The data for Ag(100) and Pd(100) are taken from Refs. [3] and [4]. For V and Ni, we see that the energy differences are small: 4 and 15 meV, respectively. Experimentally, the case of a single monolayer V on Ag(100) was discussed controversially, claiming ferromagnetic order,[38] or the absence of ferromagnetic order,[39] as well as evidence for antiferromagnetic order.[5] Therefore, we checked ΔE carefully as a function of several computational parameters, like **k**-point sampling of the temperature broadening at the Fermi level. Since several studies reported on a field-induced or field-assisted FM-to-AFM transition in FeRh films,[40] we also checked the stability of our results with respect to the influence of external electric fields. For the Fe monolayer on Rh(100), no significant change
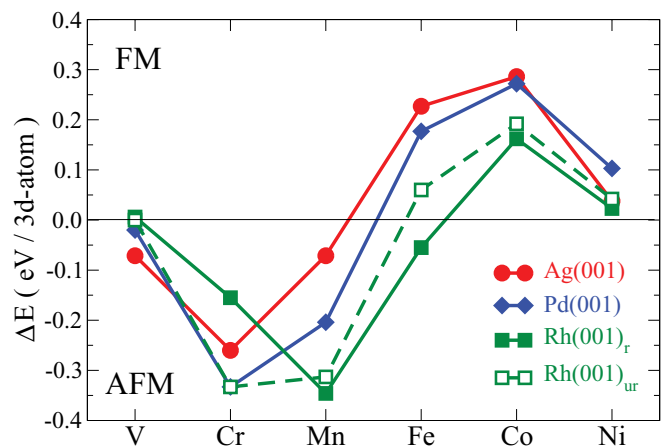

FIG. 3. (Color online) The magnetic order of 3*d* TMs on Ag, Pd, and Rh(100): positive $\Delta E = E_{AFM} - E_{FM}$ indicates a FM ground state, while negative values denote AFM order. The data for 3*d* TM on Ag(100) and Pd(100) were taken from Refs. [3] and [4]. The open squares connected with the dashed line represent the values of ΔE for the unrelaxed 3*d* TMs on Rh(100).

TABLE I. Differences of the total energy, ΔE, of the AFM and FM states for Fe monolayers on different substrates, where negative energies indicate that the AFM state is more stable. Additionally, we give the magnetic moments of Fe in the FM and the AFM state.

	ΔE (meV)	M_{FM} (μ_B)	M_{AFM} (μ_B)
Fe/Cu(100)	340	2.61	2.35
Fe/Ag(100)	210	3.01	3.06
Fe/Pd(100)	180	3.19	3.20
Fe/Rh(100)	−60	3.01	2.93
Fe/W(100)	−170	2.05	2.67

[a]The Cu(100), Ag(100), Pd(100), and W(100) data are taken from Refs. [42], [4], [41], and [6], respectively.

of the results was observed in the presence of experimentally obtainable external electric fields. From Fig. 3 we observe for V and Cr a trend toward FM order as we change the substrate from Ag or Pd to Rh, while an increasing tendency toward AFM is observed for Mn and the late TMs.

To highlight the influence of relaxations for the magnetic ground state, we also show in Fig. 3 the predicted ΔE for the unrelaxed structures: It can be noticed that, for all TMs where the relaxation for FM and AFM structures are very similar (V, Mn, Co, and Ni; see Fig. 1), relaxation effects on ΔE are rather small and do not change the predicted magnetic ground state. On the other hand, for Co and Fe we observe strong modifications of ΔE due to relaxation: In Fe, where the AFM structure shows a stronger inward relaxation than the FM structure, the ground state changes from FM toward AFM. This strong dependence of the relaxation on the magnetic structure was already noticed in Ref. 27 and a similar trend was observed for Fe on Ir(001).[14] This is not unexpected, since Rh and Ir are in the same row of the periodic table. For Cr the opposite trend in relaxation is observed and the AFM structure is destabilized. The magnetic structure that leads to the most favorable band alignment between the TM and the substrate for bonding is energetically most stable. We discuss the relations between electronic and magnetic structure in more detail in Sec. IV.

For a weakly interacting substrate, like Ag(100), the trends of ΔE can be understood on the basis of the densities of states of the TM monolayers.[41] As we move on to more strongly interacting substrates like Pd or Rh, this sinus-like curve in Fig. 3 is shifted gradually to the right; that is, hybridization with the substrate effectively lowers the d-band filling in the TM film. This trend is even more pronounced for strongly interacting early TM substrates, like W(100), causing a complete reversal of the magnetic trends.[6] A compilation of results on different substrates is presented in Table I.

C. Magnetic anisotropy

Apart from the magnetic order, the magnetic anisotropy is one of the most important quantities characterizing thin magnetic films because it not only determines the magnetization direction (in plane or out of plane) but it also leads to the stabilization of the magnetic order against thermal fluctuations in two-dimensional systems and determines as such the critical temperatures, the Néel temperature in case

of the $c(2 \times 2)$ antiferromagnets, or Curie temperature for the ferromagnets. In principle, two terms contribute to the MAE: the dipole-dipole interaction, leading in a ferromagnetic film to the magnetic shape anisotropy (MSA) and the spin-orbit coupling term giving the dominant contribution to the magnetocrystalline anisotropy (MCA). Since in ultrathin magnetic films the MCA is typically larger than the MSA, we first discuss the effects of spin-orbit coupling and add the dipole-dipole contributions at the end of this discussion. All values given here refer to the energy difference between in-plane (010) and out-of-plane (100) magnetization, positive values indicating that the latter is more stable.

To investigate the influence of the substrate on the magnetic film, we compare our results to $3d$ transition-metal unsupported monolayers (UMLs) or monolayers on weakly interacting substrates. These show on the right-hand side of the periodic table (Co, Ni) a tendency toward strong in-plane magnetization that changes to stable out-of-plane orientation at the transition from Co to Fe. Then the values of the anisotropy get smaller from Mn to V and can show small oscillations (also in sign), depending on the chosen substrate or lattice constant.[43] This tendency can also be seen for UMLs at the Rh(100) in-plane lattice constant in Fig. 4. Since the magnetic anisotropy is a small quantity, typically two orders of magnitude smaller than the energy differences between different magnetic structures (cf. Fig. 3), one might expect that hybridization effects allow these values to be manipulated considerably. As can be seen from Fig. 4, this is indeed that case, although the overall trend—as described above—remains visible.

Focusing on the case of Fe to discuss the effect of the substrate on the MCA, we first notice that both FM and AFM ordered UMLs have large out-of-plane anisotropies. Also, for Fe at the W(100) lattice constant, huge MCA values of 3.2 and 1.0 meV were reported for the AFM and FM structures, respectively.[10] On the smaller lattice constant of Rh(100) these values are smaller and the effect of hybridization with the
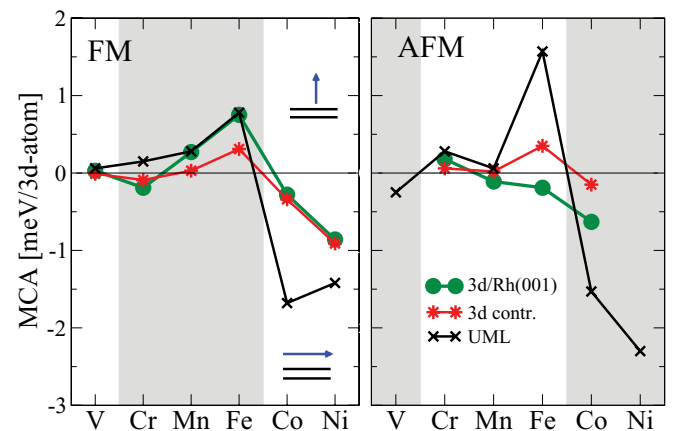

FIG. 4. (Color online) Spin-orbit contribution to the magnetocrystalline anisotropy (MCA) for one ML $3d$/Rh(100) in (left) FM and (right) AFM order. Crosses indicate the anisotropy of the unsupported monolayers, while the stars represent only the $3d$ contribution. Positive values correspond to an out-of-plane easy axis and negative values to an in-plane magnetization. The values for the magnetic ground state (FM or AFM) are shown on white background.

substrate is quite different: While the value of about 0.8 meV remains almost unchanged for FM order, in the AFM state the easy axis changes and the MCA drops to −0.2 meV due to the Rh substrate. On W(100), the opposite trend was observed: In the FM case the easy axis switched to in plane, while the AFM ordered film kept its out-of-plane easy axis also on the substrate.

In principle, two mechanisms for a reorientation of the easy axis due to the substrate are conceivable: Either the charge transfer changes the electronic properties of the TM monolayer or the SOC contribution on Rh and the induced Rh moments are responsible for the altered anisotropy. To distinguish between these effects we can exclude the influence of spin-orbit coupling in the substrate by setting the SOC matrix elements to zero in the Rh atomic spheres. The so-obtained MCA can then be attributed solely to the 3d TM atoms and is indicated by stars in Fig. 4. For Fe and the elements to the left of Fe, the charge transfer leads to a reduction of the MCA with respect to the unsupported monolayers and eventually to in-plane polarization, while for Co and Ni the opposite effect is observed. Considering further the effect of the induced Rh moments (noticing that only in the FM case moments are induced in the substrate) leads—with the exception of Cr—to an increase of the MCA. Also, with respect to the induced Rh moments, Cr is exceptional, as it induces a moment opposite to the TM layer, but it is not obvious whether there is a connection to the magnetic anisotropy. For the AFM structures, there are no induced moments, so the SOC effect on the Rh atoms can only come from small changes due to SOC in the band structure. We see that for Fe and Co this effect is quite substantial.

Finally, we note that the balance of the above-mentioned effects is quite sensitively influenced by the relaxation of the magnetic monolayers. For example, for an unrelaxed FM film of Fe on Rh, we observe just a small tendency toward an out-of-plane easy axis that is further enhanced by the relaxation of the film. The more Fe approaches the substrate, the stronger the induced magnetic moments in Rh and the more important the influence of the substrate. Additionally, the more pronounced crystal field effect from the substrate on the Fe ML tends to stabilize the out-of-plane anisotropy.[44]

Since the ground state of Cr, Mn, and Fe is AFM and for V, Co, and Ni it is FM, we observe that a (small) out-of-plane macroscopic moment is only obtained for the V overlayer. Up to now, our arguments were only based on the SOC contribution to the magnetocrystalline anisotropy, but the MAE also contains the dipole-dipole interaction, which we neglected so far. Since this interaction scales with the square of the magnetic moments, we expect it to be important in the middle of the 3d series, where films with an antiferromagnetic ground state are found. For FM films, the dipole-dipole interaction can be approximated in a continuum model, giving rise to the shape anisotropy which is for a thin film with an atomic volume V and magnetic moments m (in μ_B) given as

$$K_{\text{shape}} = -2\pi \frac{1}{2c^2} \frac{m^2}{V},$$ (2)

where atomic (Hartree) units are used and the negative sign implies that for FM films the dipole-dipole interaction favors

an in-plane easy axis. In AFM films there is no contribution from the dipole-dipole interaction in the continuum model and the dipole sum has to be carried out explicitly, where it is found that the out-of-plane direction is favored.[45] In our calculations we included also the induced magnetic moments of the substrate. Since the V moment is rather small, the dipole-dipole interaction is also tiny and the MSA adds for this FM film only −2 μeV to the MCA. For AFM structures, the dipole-dipole contribution is positive, adding for Cr and Fe about 0.10 meV and for Mn 0.15 meV to the MCA, which makes the MAE for Fe and Mn on Rh(100) small, but still negative. In the FM Co and Ni overlayers, the MSA further stabilizes the in-plane orientation of the magnetization.

In two-dimensional systems, the magnetic anisotropy is of particular importance for the stabilization of the magnetic order at finite temperatures. For example, in a system with uniaxial anisotropy it was shown that the ordering temperature in two dimensions, T_2, can be derived by a renormalization of the ordering temperature in three dimensions, T_3, according to[46]

$$T_2 = \frac{2T_3}{\ln(\pi^2 J/K)},$$ (3)

where J is the nearest-neighbor exchange coupling as defined in a Heisenberg model and K is the uniaxial anisotropy. For a square lattice with out-of-plane anisotropy, this model can be used to estimate the ordering temperature from the energy difference between FM and AFM structures (Fig. 3) and the anisotropy (Fig. 4). Since there are only two systems with out-of-plane easy axis in the ground state, V and Cr, we can focus on these two. However, for V the exchange coupling, J, and the anisotropy, K, is tiny and the Curie temperature is only 3 K. For Cr, we estimate a value of 295 K, so that the chances are good that this structure can be directly observed experimentally with a spatially nonaveraging technique.

In in-plane magnetized films, the temperature dependence of the magnetization depends on both the MAE as discussed above and the magnetic anisotropy within the plane.[47] Although these in-plane anisotropies are tiny (about 2 μeV per atom for the Fe overlayer), they are essential in stabilizing the magnetic order at low temperatures, where these values can be used to describe the temperature dependence of the magnetization within the random phase approximation. Unfortunately, the extension toward T_2 is problematic in this case.[48]

IV. DISCUSSION

To analyze the role of the hybridization between the Fe ML and the Ag, Pd, or Rh substrate, the local density of states (LDOS) for the nonmagnetic (NM) and the FM configuration of one ML Fe on different substrates are shown in Fig. 5. We see from the NM LDOS that there is no overlap of the Ag 4d band with the Fe DOS, which is pinned at the Fermi level due to its incomplete 3d band filling. Therefore, the Fe bandwidth is small and (according to the Stoner model) the high DOS at the Fermi level favors ferromagnetism. In contrast there is a strong 3d-4d hybridization between the Fe ML and the the Rh(100) substrate. The broadening of the Fe d band reduces the DOS at the Fermi level, leading finally to an
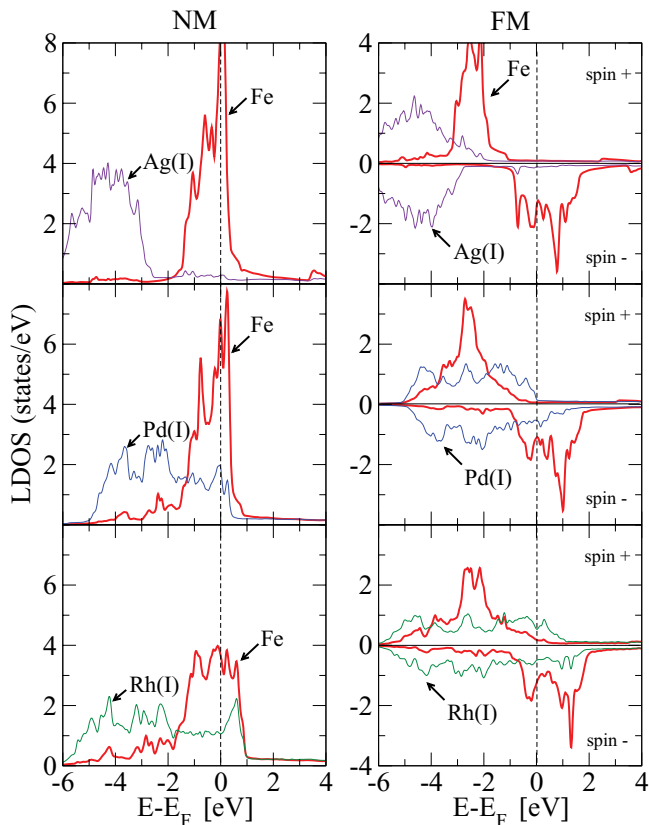
FIG. 5. (Color online) Local densities of states (LDOS) for the Fe atoms and the substrate atoms at the interface (I) for the nonmagnetic (NM) and FM configurations of Fe on Ag(100), Pd(100), and Rh(100) (top to bottom). The LDOS of the 3d metal is drawn with thick (red) lines, and the substrates' LDOS is shown with thin lines.
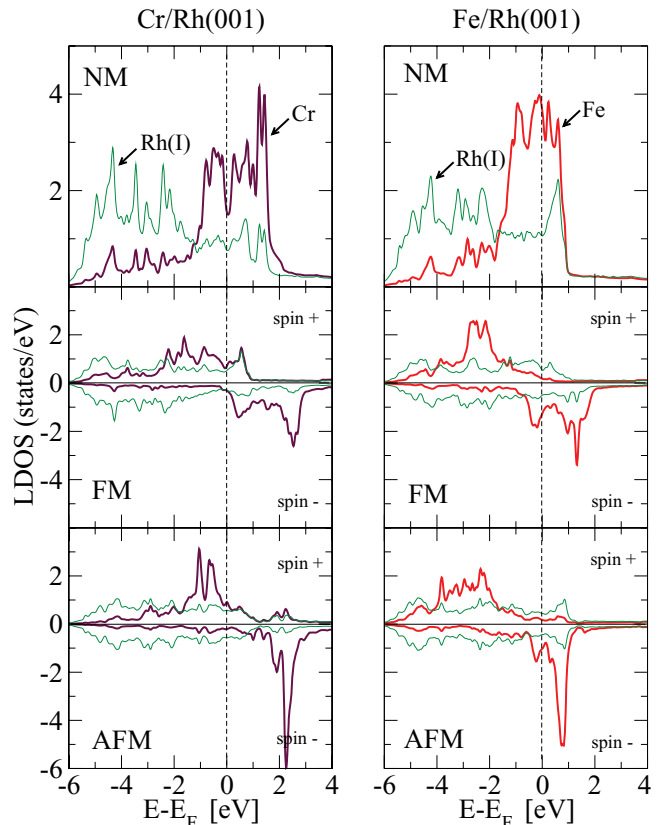

FIG. 6. (Color online) LDOS for the (top) NM, (middle) FM, and (bottom) AFM configurations of (left) Cr and (right) Fe on the Rh(100) surface. The LDOS of the 3d metal is drawn with thick lines, and the substrates' LDOS is shown with thin (green) lines.

antiferromagnetic ground state. The case of Fe/Pd(100) is in between these extremes, but still a FM order is obtained as a ground state. From the FM DOS it can be seen that a small FM moment can be induced in the Pd interface that is absent in the case of Fe/Ag(100).

Coming back to the previous discussion of the effects of bonding (relaxation) on the magnetic structure, we now compare Fe on Rh(100) to Cr/Rh(100). The fact that the latter has a strong tendency toward a $c(2 \times 2)$ AFM ground state can be explained from the NM LDOS (top of Fig. 6): We see that the Fermi level falls in a minimum of the Cr LDOS, favoring the AFM ground state even more than in the case of Fe (see Fig. 3). A comparison of the magnetic DOS shows that in Fe/Rh(100) the minority DOS is pinned at the Fermi level, while in the Cr case the position of the majority d band is determined by the band filling and the whole exchange-split d-like DOS is energetically at a much higher position. This modifies the hybridization to the substrate, as can be seen in the relaxations: While Fe and Cr have very similar bulk lattice constants, the inward relaxation of FM Cr on Rh(100) is much bigger than that of FM Fe/Rh(100) (see Fig. 1). In the case of the AFM solutions, the trend is exactly opposite; that is, Fe relaxes much more than Cr. In Cr in the AFM state, the d bandwidth is much smaller than in the FM state, leading to a decreased hybridization with the substrate. In contrast, the AFM Fe DOS can be seen to be stronger hybridized to the

Rh, so that an increase in hybridization (stronger relaxation) is connected to a stabilization of the AFM structure (Fig. 3), as opposed to the observations for the Cr ML. We should note here that in all these cases the magnetic moments (and the exchange splitting) are approximately the same (Fig. 2), so magnetovolume effects should be comparable.

V. SUMMARY

Monolayers of 3d transition metals were studied on top of a Rh(100) surface including relaxations of the topmost layers. As in the previously studied 3d TM series on Ag(100) and Pd(100), the trend of the magnetic moments follows Hund's first rule with the largest moments on Mn. Opposed to that, the largest induced magnetic moments in Rh are obtained at the end of the TM series. The magnetic order was found to be FM for V, Co, and Ni overlayers, whereas Cr, Mn, and Fe favor an AFM ground state. Depending on the substrate, Fe can be tuned from an AFM state on Rh and W to FM coupling on Pd and Ag(100). A similar behavior was reported recently for Fe on W(100) and Ta(100) surfaces: Complex magnetic structures can be expected when the nearest-neighbor exchange coupling is small, that is, when $\Delta E = E_{AFM} - E_{FM}$ is small.[49] Also, frustration effects, like on Rh(111) surfaces, could lead to interesting magnetic structures.[50] From the LDOS it can be seen how hybridization affects the magnetic order in these systems: Compared to Ag or Pd(100) substrates,

the broadening of the *d* band is enhanced, leading to a tendency in favor of AFM ordering for Fe but FM for Cr. Calculations of the magnetic anisotropy showed that only V and Cr monolayers on Rh(100) have an out-of-plane easy axis in their ground state, while the magnetization of Mn, Fe, Co, and Ni is oriented in plane.

*Present Address: Max-Planck-Institut für Eisenforschung, Düsseldorf, Germany.

†g.bihlmayer@fz-juelich.de

[1] A. J. Freeman and A. Q. Wu, J. Magn. Magn. Mater. **100**, 497 (1991).

[2] T. Asada, G. Bihlmayer, S. Handschuh, S. Heinze, Ph. Kurz, and S. Blügel, J. Phys.: Condens. Matter **11**, 9347 (1999).

[3] S. Blügel, Europhys. Lett. **7**, 743 (1988).

[4] S. Blügel and P. H. Dederichs, Europhys. Lett. **9**, 597 (1989).

[5] J. E. Ortega and F. J. Himpsel, Phys. Rev. B **47**, 16441 (1993).

[6] P. Ferriani, S. Heinze, G. Bihlmayer, and S. Blügel, Phys. Rev. B **72**, 024452 (2005).

[7] R. Wu and A. J. Freeman, Phys. Rev. B **45**, 7532 (1992).

[8] X. Qian and W. Hübner, Phys. Rev. B **60**, 16192 (1999).

[9] D. Spišák and J. Hafner, Phys. Rev. B **70**, 195426 (2004).

[10] A. Kubetzka, P. Ferriani, M. Bode, S. Heinze, G. Bihlmayer, K. von Bergmann, O. Pietzsch, S. Blügel, and R. Wiesendanger, Phys. Rev. Lett. **94**, 087204 (2005).

[11] P. Ferriani, K. von Bergmann, E. Y. Vedmedenko, S. Heinze, M. Bode, M. Heide, G. Bihlmayer, S. Blügel, and R. Wiesendanger, Phys. Rev. Lett. **101**, 027201 (2008).

[12] P. Ferriani, K. von Bergmann, E. Y. Vedmedenko, S. Heinze, M. Bode, M. Heide, G. Bihlmayer, S. Blügel, and R. Wiesendanger, Phys. Rev. Lett. **102**, 019901(E) (2009).

[13] M. Ondráček, J. Kudrnovský, and F. Máca, Surf. Sci. **601**, 4261 (2007).

[14] J. Kudrnovský, F. Máca, I. Turek, and J. Redinger, Phys. Rev. B **80**, 064405 (2009).

[15] K. von Bergmann, S. Heinze, M. Bode, E. Y. Vedmedenko, G. Bihlmayer, S. Blügel, and R. Wiesendanger, Phys. Rev. Lett. **96**, 167203 (2006).

[16] T. Kachel, W. Gudat, C. Carbone, E. Vescovo, S. Blügel, U. Alkemper, and W. Eberhardt, Phys. Rev. B **46**, 12888 (1992).

[17] G. Shirane, R. Nathans, and C. W. Chen, Phys. Rev. **134**, A1547 (1964).

[18] V. L. Moruzzi and P. M. Marcus, Phys. Rev. B **46**, 2864 (1992).

[19] K. Nakada and H. Yamada, J. Magn. Magn. Mater. **310**, 1046 (2007).

[20] C. Egawa, Y. Tezuka, S. Oki, and Y. Murata, Surf. Sci. **283**, 338 (1993).

[21] A. M. Begley, S. K. Kim, F. Jona, and P. M. Marcus, J. Phys.: Condens. Matter **5**, 7307 (1993).

[22] K. Hayashi, M. Sawada, A. Harasawa, A. Kimura, and A. Kakizaki, Phys. Rev. B **64**, 054417 (2001).

[23] K. Hayashi, M. Sawada, H. Yamagami, A. Kimura, and A. Kakizaki, J. Phys. Soc. Jpn. **73**, 2550 (2004).

[24] K. Hayashi, M. Sawada, H. Yamagami, A. Kimura, and A. Kakizaki, Phys. B (Amsterdam) **351**, 324 (2004).

[25] F. Yildiz, F. Luo, C. Tieg, R. M. Abrudan, X. L. Fu, A. Winkelmann, M. Przybylski, and J. Kirschner, Phys. Rev. Lett. **100**, 037205 (2008).

[26] F. Yildiz, M. Przybylski, and J. Kirschner, Phys. Rev. Lett. **103**, 147203 (2009).

[27] C. Hwang, A. K. Swan, and S. C. Hong, Phys. Rev. B **60**, 14429 (1999).

[28] D. Spišák and J. Hafner, Phys. Rev. B **73**, 155428 (2006).

[29] E. Wimmer, H. Krakauer, M. Weinert, and A. J. Freeman, Phys. Rev. B **24**, 864 (1981).

[30] [http://www.flapw.de].

[31] J. P. Perdew, K. Burke, and M. Ernzerhof, Phys. Rev. Lett. **77**, 3865 (1996).

[32] M. Körling and J. Häglund, Phys. Rev. B **45**, 13293 (1992).

[33] A. R. Mackintosh and O. K. Andersen, in *Electrons at the Fermi Surface*, edited by M. Springford (Cambridge University, London, 1980), p. 149 .

[34] A. M. Begley, S. K. Kim, F. Jona, and P. M. Marcus, Phys. Rev. B **48**, 1786 (1993).

[35] M. Methfessel, D. Hennig, and M. Scheffler, Phys. Rev. B **46**, 4816 (1992).

[36] S. Handschuh and S. Blügel, Solid State Commun. **10**, 633 (1998).

[37] M. A. Tomaz, E. Mayo, D. Lederman, E. Hallin, T. K. Sham, W. L. O'Brien, and G. R. Harp, Phys. Rev. B **58**, 11493 (1998).

[38] C. Rau, G. Xing, and M. Robert, J. Vac. Sci. Technol. A **6**, 1077 (1988).

[39] M. Stampanoni, A. Vaterlaus, D. Pescia, M. Aeschlimann, F. Meier, W. Dürr, and S. Blügel, Phys. Rev. B **37**, 10380 (1988).

[40] S. Maat, J.-U. Thiele, and E. E. Fullerton, Phys. Rev. B **72**, 214432 (2005).

[41] S. Blügel, M. Weinert, and P. H. Dederichs, Phys. Rev. Lett. **60**, 1077 (1988).

[42] S. Blügel, Appl. Phys. A **63**, 595 (1996).

[43] S. Blügel and G. Bihlmayer, in *Handbook of Magnetism and Advanced Magnetic Materials*, edited by H. Kronmüller and S. Parkin (Wiley, Hoboken, NJ, 2007), Vol. 1, p. 598.

[44] J. Stöhr, J. Magn. Magn. Mater. **200**, 470 (1999).

[45] P. J. Jensen, Acta Phys. Pol. A **92**, 427 (1997).

[46] R. P. Erickson and D. L. Mills, Phys. Rev. B **43**, 11527 (1991).

[47] J. A. C. Bland, G. A. Gehring, B. Kaplan, and C. Caboo, J. Magn. Magn. Mater. **113**, 173 (1992).

[48] B. Kaplan, Turk. J. Phys. **23**, 1093 (1999).

[49] P. Ferriani, I. Turek, S. Heinze, G. Bihlmayer, and S. Blügel, Phys. Rev. Lett. **99**, 187203 (2007).

[50] B. Hardrat, A. Al-Zubi, P. Ferriani, S. Blügel, G. Bihlmayer, and S. Heinze, Phys. Rev. B **79**, 094411 (2009).